Revista Mexicana de Astronomía y Astrofísica, **46**, 253–262 (2010)

COMPACT RADIO SOURCES IN THE VICINITY OF THE ULTRACOMPACT HII REGION G78.4+2.6

Citlali Neria, Yolanda Gómez, and Luis F. Rodríguez

Centro de Radioastronomía y Astrofísica
Universidad Nacional Autónoma de México, Morelia, Mexico

Received 2010 January 26; accepted 2010 June 4

RESUMEN

Utilizando el Very Large Array (VLA) a 3.6 cm, hemos identificado cuatro nuevas fuentes compactas de radio en los alrededores de la región HII con morfología cometaria G78.4+2.6 (VLA 1). Las cuatro fuentes compactas de radio (denominadas VLA 2 a 5), tienen contrapartes en el infrarrojo cercano, como se muestra en la imagen del Spitzer a 3.6 μm. Una de estas fuentes (VLA 5) claramente muestra evidencia de radio-variabilidad en una escala de tiempo de horas. Hemos explorado la posibilidad de que estas radio-fuentes están asociadas con estrellas de pre-secuencia principal (PMS) en la vecindad de la región HII ultracompacta G78.4+2.6. Nuestros resultados favorecen una distancia corta de 1.7 kpc para G78.4+2.6. Además de la detección de radio-fuentes en los alrededores de G78.4+2.6, detectamos otro grupo de cinco fuentes, localizado aproximadamente $3'$ al noroeste de la región HII. Algunas de estas fuentes presentan emisión extendida.

ABSTRACT

Using the Very Large Array (VLA) at 3.6 cm we identify four new compact radio sources in the vicinity of the cometary HII region G78.4+2.6 (VLA 1). The four compact radio sources (named VLA 2 to VLA 5), have near-infrared counterparts, as seen in the 3.6 μm Spitzer image. One of them (VLA 5) clearly shows evidence of radio variability in a timescale of hours. We explore the possibility that these radio sources are associated with pre-main sequence (PMS) stars in the vicinity of the UC HII region G78.4+2.6. Our results favor the smaller distance value of 1.7 kpc for G78.4+2.6. In addition to the detection of the radio sources in the vicinity of G78.4+2.6, we detected another group of five sources which appear located about $3'$ to the northwest of the HII region. Some of them exhibit extended emission.

Key Words: HII regions — ISM: individual (G78.4+2.6, IRAS 20178+4046) — radio continuum: stars

1. INTRODUCTION

Although our understanding of star forming regions has progressed in recent years, many aspects of the early evolution stages are still unclear. Observationally, pre-main sequence (PMS) stars are among the most difficult to study because they are usually heavily obscured by their parental molecular cloud. Observations at radio wavelengths of young clusters are of considerable relevance because a fraction of these stars appear to be undetectable even in the infrared. In this sense radio observations can provide unique information. Radio clusters of non-thermal PMS stars have been found in several star forming regions. Gómez et al. (2000, 2002) reported centimeter wavelength observations of the GGD14 star forming region. In this study, they found a radio cluster of PMS stars made of eight extremely compact and faint radio sources around a compact HII region that seems to be ionized by a B0.5 zero age main sequence (ZAMS) star. Similar radio clusters have been studied toward HH 124 IRS by Reipurth et al. (2002), NGC 2024 (Orion B) by Rodríguez,

Gómez, & Reipurth (2003) and toward the Orion Nebula (M42) by Zapata et al. (2004), among others. Some members of the radio clusters mentioned above are characterized by compact non-thermal emission, time variability, and in some cases circular polarization. All these characteristics suggest that most likely their radio emission is due to the gyrosynchrotron mechanism from an active magnetosphere in a PMS star (e.g. Gómez et al. 2002).

The identification of more such PMS clusters can provide valuable information of the star forming processes. Here we present the identification of new members that surround the HII region G78.4+2.6. This is an ultracompact (UC) HII region whose estimated kinematic distances range from 1.7 kpc (Wilking et al. 1989; Schneider et al. 2006) to 3.3 kpc (Kurtz, Churchwell, & Wood 1994). It has a cometary morphology (Kurtz et al. 1994) and it is associated with the IRAS source 20178+4046 with a far-infrared luminosity of 7×10^4 $L_\odot$ (assuming a distance of 3.3 kpc). From the radio continuum emission the HII region seems to be ionized by a B0–B0.5 ZAMS star (Kurtz et al. 1994; Tej et al. 2007). No maser emission of OH (6035 MHz), H_2O (22.2 GHz) or CH_3OH (6.7 GHz) or thermal emission of NH_3 (23.6–23.9 GHz) has been detected toward this region (Baudry et al. 1997; Codella, Felli, & Natale 1996; Kurtz & Hofner 2005; Sunada et al. 2007; Slysh et al. 1999). In the mid-infrared images the UC HII region appears single (Crowther & Conti 2003), but the presence of a stellar group/cluster around it is clear in the near-infrared images (Tej et al. 2007).

Recently, Tej et al. (2007) presented a multiwavelength study toward IRAS 20178+4046. They used the Giant Metrewave Radio Telescope (GMRT) to map the radio continuum emission at 1280 and 610 MHz. Available archival data from the Two Micron All Sky Survey (2MASS), the Midcourse Space Experiment (MSX), and the James Clerk Maxwell Telescope (JCMT) were used to study the complex in the near-infrared (NIR) JHK bands, the mid-infrared at 8.3, 12.13, 14.65 and 21.34 μm and the sub-mm at 450 and 850 μm, respectively. From their analysis of the NIR 2MASS data, they proposed the presence of nine early type sources with spectral types $\sim$ B0.5 or earlier around IRAS 20178+4046. Their multiwavelength study led Tej et al. (2007) to conclude that a scenario with possible different evolutionary stages of star formation is present toward IRAS 20178+4046 (G78.4+2.6).

In this paper we present sensitive high resolution radio continuum observations at 3.6 cm in order to search for faint compact radio continuum sources around this UC HII region.

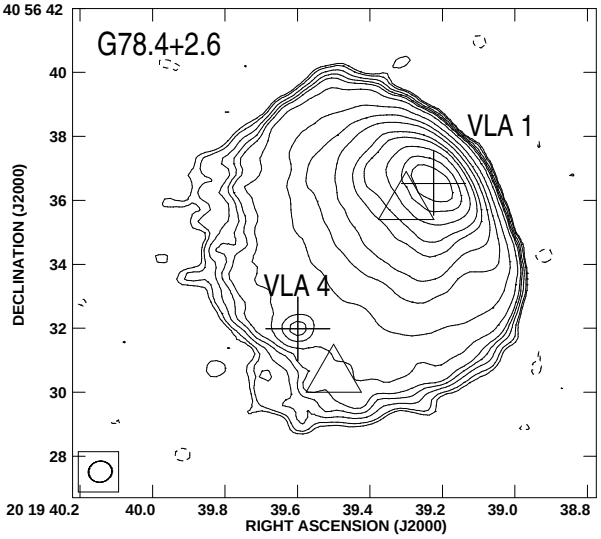

Fig. 1. Contour image of the 3.6 cm continuum emission from the UC HII region G78.4+2.6. The contours are –3, 3, 4, 6, 8, 10, 15, 30, 50, 70, 100, 120, 150, 180 and 200 times 10 μJy beam^{-1}, the rms noise of the image. The synthesized beam ($0\farcs76 \times 0\farcs67$ with a position angle of $-79°$) is shown in the bottom left corner of the image. The dynamic range achieved in the 3.6 cm image is approximately 200. The crosses mark the peak position of the 3.6 cm radio sources VLA 1 and VLA 4. The triangles mark the positions of the NIR sources number 1 (bottom left) and number 2 (top right) of Tej et al. (2007).

2. OBSERVATIONS

G78.4+2.6 was observed with the VLA of the NRAO[1] at 3.6 cm (8.4 GHz) in the B configuration during 2002 August 6 and 7 for a total on-source time of $\sim$ 10 hrs. The data were taken using two IFs each with an effective bandwidth of 50 MHz and both circular polarizations. The flux density scale was determined from observations of the amplitude calibrator 1331+305, for which we assumed a flux density of 5.22 and 5.20 Jy, for IF=1 (8.4351 GHz) and IF=2 (8.4851 GHz), respectively. The source 2007+404 was used as the phase calibrator, with bootstrapped flux densities of 2.704 ± 0.003 and 2.708 ± 0.003 Jy for the first and second IF, respectively. The data were edited and calibrated using the standard procedures of the Astronomical Image Processing System (AIPS) of NRAO. The data were also self-calibrated

[1]The National Radio Astronomy Observatory (NRAO) is operated by Associated Universities Inc. under cooperative agreement with the National Science Foundation.

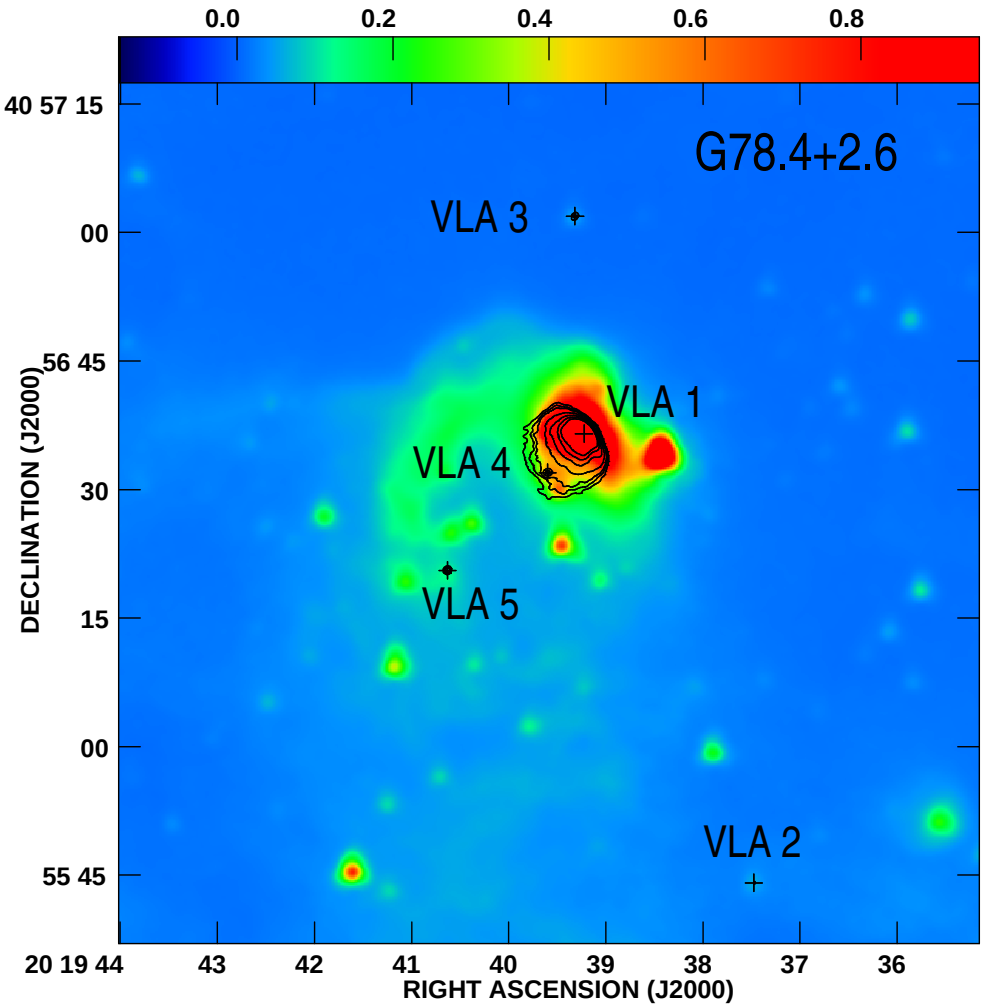

Fig. 2. The image shows the Spitzer 3.6 μm band emission in color for the region around G78.4+2.6. Color scale goes from -0.15 to 0.95 GJy sr^{-1}. The contours represent the 3.6 cm continuum emission from G78.4+2.6 showing the four compact radio sources. The contours are –5, 5, 10, 15, 30, 50, 70 and 90 times 10 μJy beam^{-1}, the average rms noise of the image. The crosses mark the peak position of the 3.6 cm radio sources listed in Table 1. The synthesized beam is $0\farcs76 \times 0\farcs67$ with a position angle of $-79°$.

in phase and for sources far away from the center we applied a primary beam correction to the images (with the task PBCOR). The synthesized beam is $0\farcs76 \times 0\farcs67$ with a position angle of $-79°$, and the rms noise is 10 μJy beam^{-1}.

3. RESULTS

3.1. *Compact radio sources toward G78.4+2.6*

Figures 1 and 2 show the radio continuum emission at 3.6 cm toward the UC HII region G78.4+2.6. In addition to the UC HII region, which we hereafter call VLA 1, it is possible to identify emission from four fainter compact radio continuum sources above the 5σ level; they are called VLA 2 through VLA 5 by us. Figure 1 shows VLA 1 and the compact source VLA 4, which appears inside the extended emission region of the cometary source VLA 1. The source VLA 4 could be physically embedded in the cometary HII region. Unfortunately, our data do not have enough angular resolution to ascertain the nature of this radio source. Figure 2 exhibits a larger area where all the compact radio sources in the vicinity of VLA 1 can be identified.

For these compact sources, we looked for near-infrared counterparts using the Spitzer 3.6 μm band image and the 2MASS Point Source Catalog (PSC), within a radius of $2''$ around each VLA source. The parameters of the radio continuum sources, and their

TABLE 1

PARAMETERS OF THE RADIO SOURCES TOWARD G78.4+2.6

Source	α(2000)	δ(2000)	Flux Density[a] (mJy)	NIR Counterpart (2MASS PSC)	Spitzer Counterpart[b] α(2000)	δ(2000)	Time Variable?
VLA 1	20 19 39.224	40 56 36.53	62.26±0.14	20193932+4056358[d]	20 19 39.12	40 56 37.84	N
VLA 2	20 19 37.475	40 55 44.11	0.06±0.02	20193748+4055441	20 19 37.48	40 55 44.14	N
VLA 3	20 19 39.318	40 57 01.91	0.11±0.02	20193931+4057018	20 19 39.34	40 57 01.85	N
VLA 4	20 19 39.599	40 56 31.98	0.48±0.02	20193949+4056305[e]	20 19 39.56	40 56 32.18	N
VLA 5	20 19 40.630	40 56 20.57	0.24±0.02[c]	–	20 19 40.64	40 56 20.19	Y

[a]Flux densities at 3.6 cm. The flux densities for sources VLA 2 to 5 were measured from an image where extended emission was suppressed using only (u, v) data with baselines larger than 100 kλ.

[b]Peak position associated with the 3.6 μm Spitzer image.

[c]Time-averaged flux density.

[d]NIR source number 2 of Tej et al. (2007).

[e]NIR source number 1 of Tej et al. (2007).

possible counterparts, are listed in Table 1. Of the nine NIR 2MASS sources reported by Tej et al. (2007), only one (source 2) clearly coincides in position with a VLA source (VLA 1). There is another NIR source reported by Tej (source number 1) that could be associated with a VLA source (VLA 4; within 1.″5). In Figure 1 we plot the peak position of the NIR source number 1 of Tej et al. (2007), where the shift in position with respect to the radio source VLA 4 is evident. Further observations at different frequencies and higher angular resolution are required to confirm or reject the association. Tej et al. (2007) have noted that their NIR source number 1 coincides in position with the source IRAS 20178+4046, one of the brightest infrared sources in the region.

To study the time-variability of the four fainter compact radio continuum sources (see Figure 2) during the approximately 12 hours of the total observing session (of which 10 hours were on-source), we proceeded as follows. The precise position of each source was determined from the image shown in Figure 2. The (u, v) data were then recentered at the position of the source considered and the real and imaginary parts of its flux density were plotted as a function of time, averaged over the (u, v) plane and in 10 time bins. A detailed description of this technique is given in the Appendix A. To avoid contamination from extended emission, we use only (u, v) data with baselines larger than 100 kλ, suppressing emission from scales larger than $\sim$ 0.″5. The technique did not work in a reliable way in the case of VLA 4, which is embedded in the much brighter UC HII (VLA 1). In the case of the remaining sources, we found clear evidence of variability for VLA 5. In Figure 3 we show the real and imaginary parts of its flux density as a function of time, where it can be appreciated that the source was very weak during the first half of the run and that, in a timescale of about an hour, it rose to a much stronger flux density. No evidence of variability was found for VLA 2 and VLA 3. In the last column of Table 1, we list if the sources were time-variable or not.

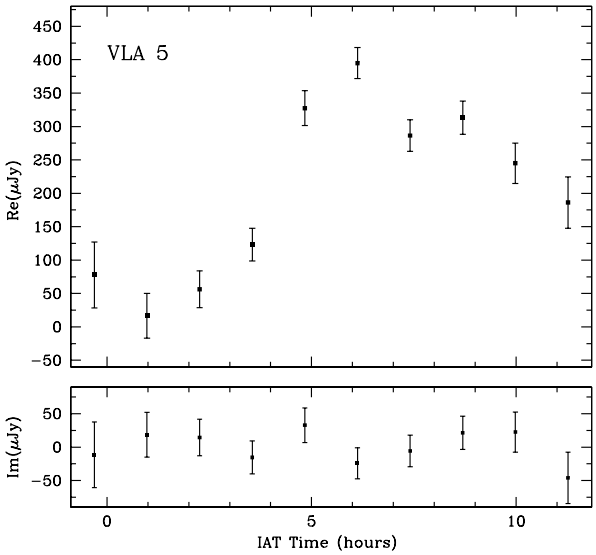

Fig. 3. Real (top) and imaginary (bottom) components of the flux density of VLA 5 as a function of time (IAT = International Atomic Time).

The variability observed in VLA 5 has been observed in other low-mass PMS stars (e.g., Gómez et

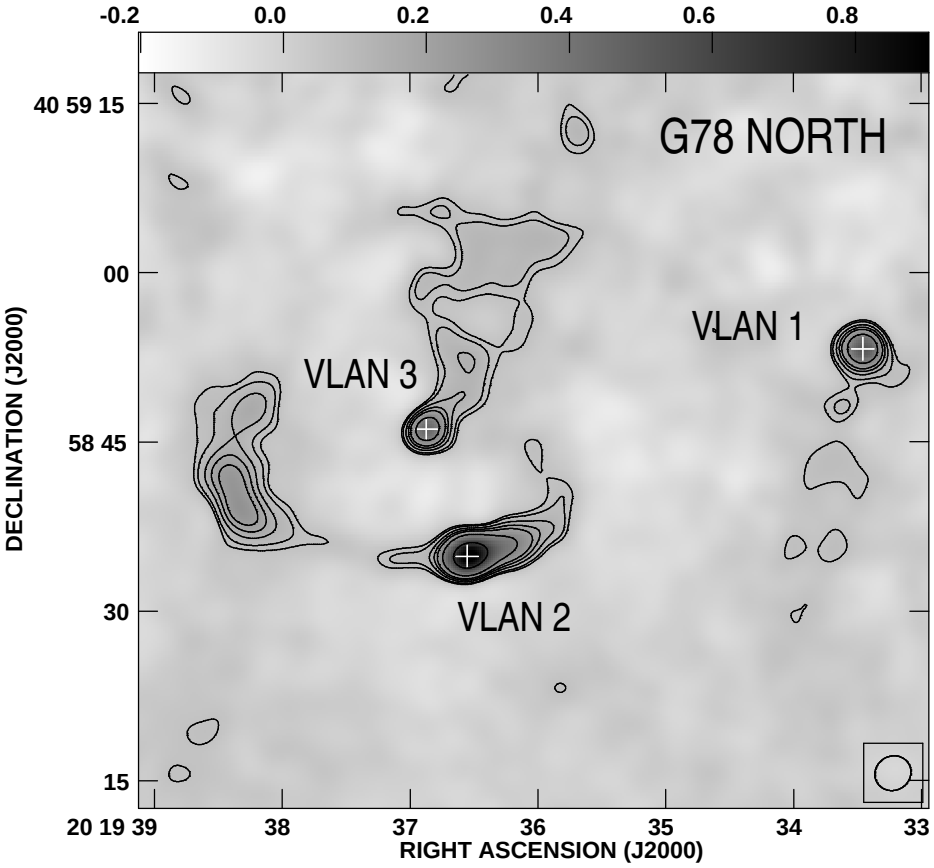

Fig. 4. Contour image overlapped on a grayscale image at 3.6 cm of VLAN 1, VLAN 2 and VLAN 3 toward the G78-North region. Contour levels are 3, 4, 6, 8, 10, 15, 30 and 50 times 21.8 μJy beam^{-1}, the average rms noise of the image. The grayscale flux goes from -0.2 to 0.9 mJy beam^{-1}. The synthesized beam, after applying UVTAPER = 50 kλ ($3\farcs26 \times 3\farcs02$ with a position angle of -60°), is shown in the bottom right corner of the image. The crosses mark the peak position of the 3.6 cm radio sources listed in Table 2.

al. 2002; Bower et al. 2003; Gómez et al. 2008; Forbrich, Menten, & Reid 2008) and it can be attributed to gyrosynchrotron emission from an active magnetosphere. For UC HII regions or externally-ionized globules variability at such short time scales is not expected.

3.2. *Other radio sources in the field*

Toward the north of the UC HII region G78.4+2.6, we detect another cluster of five compact radio sources (designated as VLAN 1 to VLAN 5) above 5σ level. After we applied UVTAPER (50 kλ, resulting in a beam size of $3\farcs26 \times 3\farcs02$, P.A. $= -60^\circ$) to this image we noted that two of these sources (VLAN 2 and 3) have diffuse extended emission associated with them. The extended radio emission toward the east of VLAN 2 is more likely an extension of a possible jet. VLAN 1 also displays some signs of extended emission though the morphology is more compact. Figure 4 shows a close-up of the north region showing these three radio sources. The compact sources VLAN 4 and VLAN 5 were not included in this close-up, because they do not exhibit significant extended emission and lie far away from the main group ($> 10''$). Figure 5 shows the sources VLAN 4 and VLAN 5. As for the four fainter compact radio continuum sources in the vicinity of the UC HII (VLA 2 to 5), we also looked for any counterparts in order to gain understanding about their nature. The search in the Strasbourg Astronomical Data Center (CDS) and the Spitzer 3.6 μm band image does not show any counterpart within one arcsec. We also searched for 1.4 GHz radio emission using the NRAO VLA Sky Survey (NVSS), which does not show any source above ~ 1.2 mJy (3σ). The morphology of VLAN 1 to 3 resembles that of a cluster of radio galaxies, but the extended emission could alternatively be HII regions surrounding massive stars.

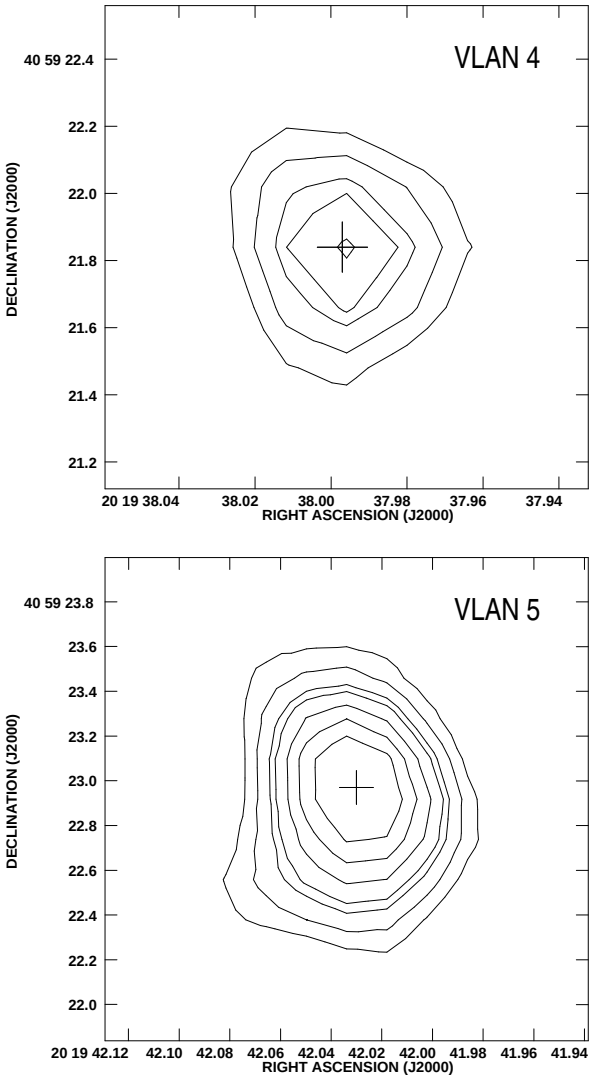

Fig. 5. Contour image of the 3.6 cm continuum emission from VLAN 4 (top) and VLAN 5 (bottom) toward the G78-North region. The contours are −5, 5, 7, 9, 10, 12, 14 and 16 times 10 μJy beam^{-1}, the average rms noise of the image. The synthesized beam is $0\farcs76 \times 0\farcs67$, with a position angle of $-79°$. The crosses mark the peak position of the 3.6 cm radio sources listed in Table 2.

Such varied morphologies of HII regions are not uncommon (e.g., Kurtz et al. 1994, 1999). However, more observations are needed in order to clarify the nature of these sources. The main parameters of the five compact radio sources to the north of G78.4+2.6 are listed in Table 2.

4. DISCUSSION

The high sensitivity continuum observations toward the region G78.4+2.6 (IRAS 20178+4046), have resulted in the identification of four new compact radio sources in the vicinity ($< 1'$) of the cometary HII region (VLA 1) (see Table 1). These sources could be associated with pre-main sequence (PMS) stars, but multiwavelength observations are required to confirm this.

TABLE 2

PARAMETERS OF THE RADIO SOURCES TOWARD THE NORTH OF G78.4+2.6

Source	α(2000)	δ(2000)	Flux Density[a] (mJy)
VLAN 1	20 19 33.457	40 58 53.25	0.57 ± 0.05
VLAN 2	20 19 36.554	40 58 34.86	0.87 ± 0.04
VLAN 3	20 19 36.874	40 58 46.14	0.49 ± 0.04
VLAN 4	20 19 37.997	40 59 21.84	0.09 ± 0.03
VLAN 5	20 19 42.030	40 59 22.97	0.28 ± 0.05

[a]Flux densities at 3.6 cm corrected for the primary beam response.

Tej et al. (2007), based on the analysis of the 850 μm emission, have reported the presence of two regions at different evolutionary stages toward this star-forming region, the northern and southern cores. The southern core traces a later stage of evolution and is associated with the UC HII region, and an earlier stage of evolution is proposed for the northern core, which does not have radio or NIR emission. Tej et al. (2007) have analyzed the nature of the near-infrared sources detected in the 2MASS JHK observations around the UC HII G78.4+2.6 region and, by using color-magnitude diagrams and assuming a distance of 3.3 kpc (Kurtz et al. 1994), they proposed the presence of nine B0.5 or earlier type candidates, all mainly located toward the southern core. However, only one (VLA) of the five radio sources reported by us in this paper (Table 1) clearly coincides in position with one of the nine B0.5 or earlier type sources proposed by Tej et al. (2007).

The UC HII region (VLA 1) is excited at least by a B0.5 ZAMS star (see discussion below) and radio emission is clearly detected. We believe that if more B0.5 stars were present in the surroundings they should have been detected in our deep radio image. The non-detection of the rest of the NIR sources could be due to a factor already considered by Tej et al. (2007): there is considerable uncertainty in the distance to G78.4+2. Indeed, if instead of the large value of 3.3 kpc we consider the smaller value of 1.7 kpc (Wilking et al. 1989; Schneider et al. 2006) then the B0.5 candidates will become less luminous stars, with no expected detectable HII region.

In the particular case of VLA 4, if it is associated with the NIR source number 1 of Tej et al. (2007), and the radio continuum reported in this work at 3.6 cm is produced by an optically thin homogeneous spherical HII region, following Mezger & Henderson (1967), we can estimate the number of ionizing photons per second, $N_{\rm i}$, produced by the exciting star as,

$$\left[\frac{N_{\rm i}}{\rm s^{-1}}\right] = 7.7\ \times 10^{43}\left[\frac{S_\nu}{\rm mJy}\right]\left[\frac{\nu}{\rm GHz}\right]^{0.1}\left[\frac{D}{\rm kpc}\right]^2,$$

where S_ν is the flux density of the compact source, ν is the observing frequency and D is the distance from the Sun. Adopting a distance of 1.7 kpc, we estimate for VLA 4 $N_{\rm i} = 1.3 \times 10^{44}$ s^{-1}, implying an exciting star type B3 ZAMS (Panagia 1973), while for a distance of 3.3 kpc, $N_{\rm i} = 5.0 \times 10^{44}$ s^{-1}, then the spectral type will be $\sim$ B2 ZAMS. In both cases the exciting star for the VLA 4 source should be later than a B2 ZAMS and does not reach the ionizing rate of a B0.5 ZAMS or earlier star. As mentioned above, Tej et al. (2007) had already pointed out that there is a discrepancy seen in their determination of the spectral types by using the NIR color-magnitude diagrams due to the distance uncertainty, to the possible presence of IR excess and to the 2MASS resolution limit.

It is possible to plot the $(H-K)$ colors and K magnitudes from our VLA sources with NIR counterparts in a color-magnitude diagram to derive the spectral types of the sources in the same way as was done by Tej et al. (2007). Assuming that VLA 1 is ionized by the NIR source number 2 of Tej et al. (2007), a B0.5 ZAMS star at a distance of 1.7 kpc is needed to provide the ionization. Then, if we apply a similar distance correction in the color-magnitude diagram (Figure 3 of Tej et al. 2007) for all the other sources, we find that VLA 4 (source number 1 of Tej) is associated with a B3 ZAMS star (consistent with our previous estimate from the radio continuum flux density). VLA 2 and VLA 3 will correspond to a spectral type between F and G ZAMS. Only one source clearly shows evidence of fast (hours) radio variability (VLA 5), a physical characteristic of low-mass PMS stars. Unfortunately, this source does not have a NIR counterpart, although it does have a Spitzer (mid-infrared) counterpart (see Table 1). We then propose that VLA 1 is an HII region excited by a B0.5 ZAMS star, VLA 4 is possibly an HII region excited by a B3 ZAMS star and that the remaining three compact radio sources (VLA 2, VLA 3 and VLA 5) are low-mass PMS stars embedded in the star forming region.

The non-detection in our data of radio continuum counterparts to the NIR sources number 3 to 9 from Tej et al. (2007), favors the smaller value of 1.7 kpc fot the distance to G78.4+2.6. Also we notice that four of our radio sources are located toward the southern core, where radio and 3.6 μm emission is present (see Figure 2), which suggests their association with a later evolutionary stage core where massive stars have formed an UC HII region.

The compact radio source VLA 3 is displaced $\sim 16''$ from the center of the northern core. The northern core is traced by the submillimeter emission at 850 μm (see Figure 5 of Tej et al. 2007) and it is not associated with radio or NIR emission, suggesting an early stage of evolution (Klein et al. 2005; Tej et al. 2006, 2007). We propose that VLA 3 may be a PMS star embedded in the early evolutionary stage northern core. Alternatively, VLA 3 could simply be an outer component of the southern core that appears projected in the line-of-sight toward the northern core. If the association with the northern core is confirmed, it will support the idea that the less massive objects are among the first ones to form in a cluster (Klein et al. 2005; Molinari et al. 2008).

In order to be sure that the four compact radio sources identified in this paper are new members of the PMS cluster toward G78.4+2.6 and not background sources, we now estimate the number count probability following Windhorst et al. (1993). The expected number of background sources per square arcmin, N, with a flux density at 8.3 GHz above S, is given by

$$\left[\frac{N}{(\rm arcmin)^2}\right] = 0.0024\left[\frac{S}{\rm mJy}\right]^{-1.3}.$$

Using $S = 0.05$ mJy (5σ of the radio continuum image), within a solid angle of $1\farcm5 \times 1\farcm5$ we obtain that the expected number of background sources is ~ 0.3, which suggests that the four compact radio sources are members of the star forming region.

Finally, following the formulation of Mezger & Henderson (1967) and Rodríguez et al. (1980) for a homogeneous and spherically symmetric region, we estimate the physical parameters of the UC HII region G78.4+2.6, assuming that the gas has constant electron density, an electron temperature of 8000 K (Tej et al. 2007) and a kinematic distance of 1.7 kpc. At 3.6 cm we measure a total flux density of ~ 62.3 mJy (see Table 1), and an angular size of $4\farcs5 \times 3\farcs5$ (~ 0.03 pc at a distance of 1.7 kpc). This flux density is in agreement with other radio estimates (Wilking et al. 1989; McCutcheon et al. 1991; Kurtz et al. 1994; Tej et al. 2007) in the 0.6–

8.5 GHz frequency range, which is consistent with an optically thin region. Under these conditions we estimate an electron density $n_e = 6.4 \times 10^3$ cm^{-3}, an ionized mass $M_{\rm HII} = 8.5 \times 10^{-3}\ M_\odot$, and an emission measure EM of 1.3×10^6 cm^{-6} pc. Using the ionizing rates of Panagia (1973) and assuming that the logarithm of the ionizing rate has an approximate linear behavior with the spectral subtype (Vacca, Garmany, & Shull 1996), we estimate for the ionizing star of VLA 1 a spectral type of B0.5 ZAMS (for a distance of 1.7 kpc) or of B0.3 ZAMS (for a distance of 3.3 kpc). The latter result is in agreement with Kurtz et al. (1994) and Tej et al. (2007) who estimated a spectral type for the exciting source of VLA 1 between B0 and B0.5 (assuming a distance of 3.3 kpc).

5. CONCLUSIONS

We present high angular resolution VLA observations at 3.6 cm toward the star-forming region G78.4+2.6. In addition to the cometary UC HII region VLA 1, a group of four compact radio sources was found (VLA 2 to 5). One of them (VLA 5) shows evidence of radio variability in a timescale of hours. The four new compact radio sources, reported by us, coincide in position with Spitzer 3.6 μm peaks. From the five radio sources reported at 3.6 cm, one is clearly associated with the NIR source number 2 of Tej et al. (2007) with a spectral type B0.5. Another VLA source (VLA 4) seems to be associated with the NIR source number 1 of Tej et al. (2007) and corresponds to a spectral type B3 ZAMS star. The rest of the radio sources (VLA 2, VLA 3 and VLA 5) are probably PMS stars with spectral types between F and G ZAMS. Our results favor the smaller distance of 1.7 kpc (Wilking et al. 1989; Schneider et al. 2006) proposed for the star forming region G78.4+2.6.

Another group of five radio sources is found about 3′ to the NW of the HII region G78.4+2.6 whose nature is still undetermined.

We thank an anonymous referee for comments and suggestions that helped to improve this paper. CN, YG, and LR are thankful for the support of DGAPA, Universidad Nacional Autónoma de México, and of Conacyt (Mexico). This research has made use of the SIMBAD database, operated at CDS, Strasbourg, France. This publication has also made use of the Spitzer Space Telescope and NASA/IPAC Infrared Science Archive, which is operated by the Jet Propulsion Laboratory, California Institute of Technology, under contract with the National Aeronautics and Space Administration.

APPENDIX A. MEASURING THE FLUX DENSITY AS A FUNCTION OF TIME IN THE (u, v) PLANE

In some cases, the observer is interested in determining the flux density of a source in the field as a function of time. This can be achieved by making images from data on small time intervals, but it is faster (since no images have to be made) to explore in the (u, v) plane different time intervals to search for variability at different timescales. As it is the case in the image plane (x, y), it is possible to isolate the emission from a source also in the (u, v) plane, as described below.

The visibility $V(u, v)$ for a given point (u, v) is (Thompson, Moran, & Swenson 1986):

$$V(u,v) = \int_{-\infty}^{+\infty}\int_{-\infty}^{+\infty} I(x,y)\exp[i2\pi(ux+vy)]dxdy\,, \tag{A1}$$

where $V(u, v)$ is the visibility, in general a complex function, u and v are the projections of the baseline of a given antenna pair along the sky coordinates x and y, respectively, given in units of wavelengths, and $I(x, y)$ is the intensity of the source or sources as a function of the position (x, y) with respect to the phase center. A point source located at the phase center, $(x, y) = (0, 0)$, can be described by

$$I(x,y) = S\ \delta^2(x,y)\,, \tag{A2}$$

where S is the flux density of the source and δ^2 is Dirac's delta function in two dimensions. The integral of equation (1) then becomes:

$$V(u,v) = S\,. \tag{A3}$$

In this case, the real, Re(u), and imaginary, Im(u), parts of the visibility are given by:

$$\mathrm{Re}(u,v) = S\,, \tag{A4}$$

$$\mathrm{Im}(u,v) = 0\,. \tag{A5}$$

Finally, the real and imaginary parts are averaged over the range of values of u and v for which one has measurements, $-u_m \le u \le u_m$, $-v_m \le v \le v_m$:

$$\mathrm{Re} = \frac{1}{2u_m}\frac{1}{2v_m}\int_{-u_m}^{+u_m}\int_{-v_m}^{+v_m}\mathrm{Re}(u,v)du\ dv = S\,, \tag{A6}$$

$$\mathrm{Im} = \frac{1}{2u_m}\frac{1}{2v_m}\int_{-u_m}^{+u_m}\int_{-v_m}^{+v_m}\mathrm{Im}(u,v)du\ dv = 0\,. \tag{A7}$$

That is, the average over (u, v) of the real and imaginary components of the visibility of a point

source at the phase center are simply S and 0, respectively.

What happens if there is an additional source in the field, that is centered at a position different from the phase center? Assuming again that this source is pointlike and that it is located at the point $(x, y) = (x_1, 0)$, it can be described by

$$I(x, y) = S_1 \ \delta^2(x - x_1, y)\,, \tag{A8}$$

where S_1 is its flux density. Again using equation (1) we have that the real, $\mathrm{Re}_1(u, v)$, and imaginary, $\mathrm{Im}_1(u, v)$, parts of the visibility are in this case given by:

$$\mathrm{Re}_1(u, v) = S_1 \ \cos(2\pi u x_1)\,, \tag{A9}$$

$$\mathrm{Im}_1(u, v) = S_1 \ \sin(2\pi u x_1)\,. \tag{A10}$$

Averaging over (u, v), we obtain

$$\begin{aligned}\mathrm{Re}_1 &= \frac{1}{2u_m}\frac{1}{2v_m}\int_{-u_m}^{+u_m}\int_{-v_m}^{+v_m}\mathrm{Re}_1(u, v)dudv \\ &= \frac{1}{2u_m}\int_{-u_m}^{+u_m} S_1 \ \cos(2\pi u x_1)du \\ &= S_1 \ \frac{\sin(2\pi u_m x_1)}{2\pi u_m x_1} = S_1 \ \mathrm{sinc}(2\pi u_m x_1)\,, \end{aligned} \tag{A11}$$

where $\mathrm{sinc} = (\sin \ x)/x$,

$$\begin{aligned}\mathrm{Im}_1 &= \frac{1}{2u_m}\frac{1}{2v_m}\int_{-u_m}^{+u_m}\int_{-v_m}^{+v_m}\mathrm{Im}_1(u, v)dudv \\ &= \frac{1}{2u_m}\int_{-u_m}^{+u_m} S_1 \ \sin(2\pi u x_1)du = 0\,. \end{aligned} \tag{A12}$$

We conclude that, in this case, the average over (u, v) of the imaginary component is 0, as in the previous case of the source at the phase center. The real component is now the flux density of the source, multiplied by a sinc function. For a well-designed interferometer we can assume that $u_m \simeq v_m$, and that the angular resolution of the data is given approximately by

$$\theta \simeq \frac{1}{u_m} \simeq \frac{1}{v_m}\,. \tag{A13}$$

We then conclude that as long as this source is several resolution elements away from the phase center and is not very bright, its contribution to the real component is small. In brief, as long as the condition

$$S \gg \frac{S_1}{2\pi(x_1/\theta)}\,, \tag{A14}$$

is fulfilled, we can take the real component of the averaged visibility as dominated by the flux density of the source at the phase center.

In the case of the source VLA 5, we have that $S \simeq 0.1 - 0.3$ mJy. The other compact sources in the field of G78.4+2.6 have flux densities comparable to that of VLA 5 and are at angular distances of $15''$ or more away from it. Since the angular resolution of the data is $\theta \simeq 0\farcs7$, we have that the angular separation is $x_1 \simeq \ 20\,\theta \simeq 20/u_m$, and that an upper limit to the contribution of these sources is given by

$$|\mathrm{Re}_1| \leq 0.003 \ \mathrm{mJy}\,. \tag{A15}$$

So, the other point sources in the field contribute less than 1% to the real component measured after centering the (u, v) data at the position of VLA 5.

We have, however, to consider the effect of the extended source VLA 1, that is quite bright, $S_1 \simeq 60$ mJy. In this case it can be shown that the condition given by equation (14) approximately becomes

$$S \gg \left[\frac{\theta}{\theta_S}\right]^2 \frac{S_1}{2\pi(x_1/\theta)}\,, \tag{A16}$$

where S_1 is the flux density of the extended source, and θ_S is its angular diameter, $\theta_S \simeq 4''$ in the case of VLA 1. In this case $x_1 \simeq 20''$. Evaluating the contribution of VLA 1 at the position of VLA 5 we obtain

$$|\mathrm{Re}_1| \leq \ 0.01 \ \mathrm{mJy}\,, \tag{A17}$$

$$\mathrm{Im}_1 = \ 0\,. \tag{A18}$$

We then conclude that the contribution of VLA 1 at the position of VLA 5 does not affect significantly the flux density determinations of the latter source. The contribution of extended sources in the field is further suppressed by not including in the averaging the short baselines of the (u, v) data, where most of the extended emission is present.

REFERENCES

Baudry, A., Desmurs, J. F., Wilson, T. L., & Cohen, R. J. 1997, A&A, 325, 255

Bower, G. C., et al. 2003, ApJ, 598, 1140

Codella, C., Felli, M., & Natale, V. 1996, A&A, 311, 971

Crowther, P. A., & Conti, P. S. 2003, MNRAS, 343, 143

Forbrich, J., Menten, K. M., & Reid, M. J. 2008, A&A, 477, 267

Gómez, Y., Rodríguez, L. F., & Garay, G. 2000, ApJ, 531, 861

_____. 2002, ApJ, 571, 901

Gómez, L., Rodríguez, L. F., Loinard, L., Lizano, S., Allen, C., Poveda, A., & Menten, K. M. 2008, ApJ, 685, 333

Klein, R., Posselt, B., Schreyer, K., Forbrich, J., & Henning, T. 2005, ApJS, 161, 361
Kurtz, S., Churchwell, E., & Wood, D. O. S. 1994, ApJS, 91, 659
Kurtz, S., & Hofner, P. 2005, AJ, 130, 711
Kurtz, S. E., Watson, A. M., Hofner, P., & Otte, B. 1999, ApJ, 514, 232
McCutcheon, W. H., Sato, T., Dewdney, P. E., & Purton, C. R. 1991, AJ, 101, 1435
Mezger, P. G., & Henderson, A. P. 1967, ApJ, 147, 471
Molinari, S., Pezzuto, S., Cesaroni, R., Brand, J., Faustini, F., & Testi, L. 2008, A&A, 481, 345
Panagia, N. 1973, AJ, 78, 92
Reipurth, B., Rodríguez, L. F., Anglada, G., & Bally, J. 2002, AJ, 124, 1045
Rodríguez, L. F., Gómez, Y., & Reipurth, B. 2003, ApJ, 598, 1100
Rodríguez, L. F., Moran, J. M., Ho, P. T. P., & Gottlieb, E. W. 1980, ApJ, 235, 845
Schneider, N., et al. 2006, A&A, 458, 855
Slysh, V. I., Val'tts, I. E., Kalenskii, S. V., Voronkov, M. A., Palagi, F., Tofani, G., & Catarzi, M. 1999, A&AS, 134, 115
Sunada, K., Nakasato, T., Ikeda, N., Hongo, S., Kitamura, Y., & Yang, J. 2007, PASJ, 59, 1185
Tej, A., Ghosh, S. K., Kulkarni, V. K., Ojha, D. K., Verma, R. P., & Vig, S. 2007, A&A, 468, 1001
Tej, A., Ojha, D. K., Ghosh, S. K., Kulkarni, V. K., Verma, R. P., Vig, S., & Prabhu, T. P. 2006, A&A, 452, 203
Thompson, A. R., Moran, J. M., & Swenson, G. W. 1986, Interferometry and Synthesis in Radio Astronomy (New York: Wiley-Interscience)
Vacca, W. D., Garmany, C. D., & Shull, J. M. 1996, ApJ, 460, 914
Wilking, B. A., Blackwell, J. H., Mundy, L. G., & Howe, J. E. 1989, ApJ, 345, 257
Windhorst, R. A., Fomalont, E. B., Partridge, R. B., & Lowenthal, J. D. 1993, ApJ, 405, 498
Zapata, L., Rodríguez, L. F., Kurtz, S., & O'Dell, C. R. 2004, ApJ, 127, 2252

Citlali Neria, Yolanda Gómez, and Luis F. Rodríguez: Centro de Radiostronomía y Astrofísica, Universidad Nacional Autónoma de México, Apdo. Postal 3-72 (Xangari), 58089 Morelia, Michoacán, Mexico (c.neria, y.gomez, l.rodriguez@crya.unam.mx).